



## Dynamical (e,2e) investigations of tetrahydrofuran and tetrahydrofurfuryl alcohol as DNA analogues

D.B. Jones<sup>a,\*</sup>, J.D. Bult-Williams<sup>b</sup>, S.M. Bellm<sup>b</sup>, L. Chiari<sup>b</sup>, H. Chaluvadi<sup>c</sup>, D.H. Madison<sup>c</sup>, C.G. Ning<sup>d</sup>, B. Lohmann<sup>e</sup>, O. Ingólfsson<sup>f</sup>, M.J. Brunger<sup>b,g,\*</sup>

<sup>a</sup>School of Chemical and Physical Sciences, Flinders University, GPO Box 2100, Adelaide, South Australia 5001, Australia

<sup>b</sup>ARC Centre of Excellence for Antimatter-Matter Studies, Flinders University, GPO Box 2100, Adelaide, South Australia 5001, Australia

<sup>c</sup>Department of Physics, Missouri University of Science and Technology, Rolla, MO 65409, USA

<sup>d</sup>Department of Physics, State Key Laboratory of Low-Dimensional Quantum Physics, Tsinghua University, Beijing 100084, China

<sup>e</sup>University of the Sunshine Coast, Maroochydore DC, Queensland 4558, Australia

<sup>f</sup>Department of Chemistry and Science Institute, University of Iceland, Dunhagi 3, 107 Reykjavik, Iceland

<sup>g</sup>Institute of Mathematical Sciences, University of Malaya, 50603 Kuala Lumpur, Malaysia

### ARTICLE INFO

#### Article history:

Received 25 February 2013

In final form 12 April 2013

Available online 20 April 2013

### ABSTRACT

Triple differential cross section measurements for the electron-impact ionization of the highest occupied molecular orbital of tetrahydrofuran (THF) are reported. Experimental measurements were performed using the (e,2e) technique in asymmetric coplanar kinematics with an incident electron energy of 250 eV and an ejected electron energy of 20 eV. With the scattered electrons being detected at  $-5^\circ$ , the angular distribution of the ejected electrons was observed. These measurements are compared with calculations performed within the molecular 3-body distorted wave (M3DW) model, and against previous measurements on THF and tetrahydrofurfuryl alcohol to further understand the role that kinematics and structure play in electron-impact ionization.

© 2013 Elsevier B.V. All rights reserved.

### 1. Introduction

There have been a number of recent studies on positron-induced and electron-induced phenomena in biologically relevant molecules (see [1,2] and references therein). This stems from the fact that such studies are required to develop models to simulate charged-particle induced damage to biological systems. Electron scattering is particularly important in this sense, as a large number of low-energy secondary electrons (LESEs) are produced from a single high-energy ionizing particle [3], and these, in turn, can efficiently induce DNA damage through single and double strand breakages [4]. Further, such damage has been found to result from localized electron-interactions with the sub-units of DNA, rather than the bulk structure [5,6]. This has created a pressing need to characterize the electron scattering mechanisms for key structural moieties found in biological systems. Of particular importance is substantiated knowledge of the electron-impact cross sections that describe the probability of the electron-induced scattering phenomena. Here experimental and theoretical cross sections are

particularly useful in simulating charged-particle interactions in the media resembling biological systems.

Given the complex composition of DNA and other biologically relevant compounds, it is clear, that if charged-particle induced damage in these macro-molecules is to be accurately simulated, we need to identify and understand the role of isolated chemical structures within them. In this context, it is also particularly important to identify the most suitable model compounds that can allow for accurate simulations of the radiation induced DNA damage facilitated by LESEs.

In an effort to provide a better understanding of the role of molecular structure in electron scattering dynamics we have thus expanded some recent studies on electron-impact ionization of individual biomolecules such as water [7], formic acid [8], pyrimidine [9] and thymine [10] by performing an investigation on the ionization of the structurally-related compounds tetrahydrofuran (THF) and tetrahydrofurfuryl alcohol (THFA). In this respect, an understanding of the sensitivity of the scattering behavior from specific species over a range of kinematical conditions is also pertinent.

In this Letter we consider electron-impact ionization of THF and THFA as both of these molecules resemble structural units of the phosphate deoxyribose backbone of DNA (see Figure 1). Indeed, this fact has led to a number of recent studies of electron scattering phenomena from both THF and THFA, which included measurements of electron-impact total [11–15], elastic [15–21] and inelastic [21–23]

\* Corresponding authors. Fax: +61 8 8201 2905 (D.B. Jones). Address: ARC Centre of Excellence for Antimatter-Matter Studies, Flinders University, GPO Box 2100, Adelaide, South Australia 5001, Australia. Fax: +61 8 8201 2905 (M.J. Brunger).

E-mail addresses: [darryl.jones@flinders.edu.au](mailto:darryl.jones@flinders.edu.au) (D.B. Jones), [michael.brunger@flinders.edu.au](mailto:michael.brunger@flinders.edu.au) (M.J. Brunger).

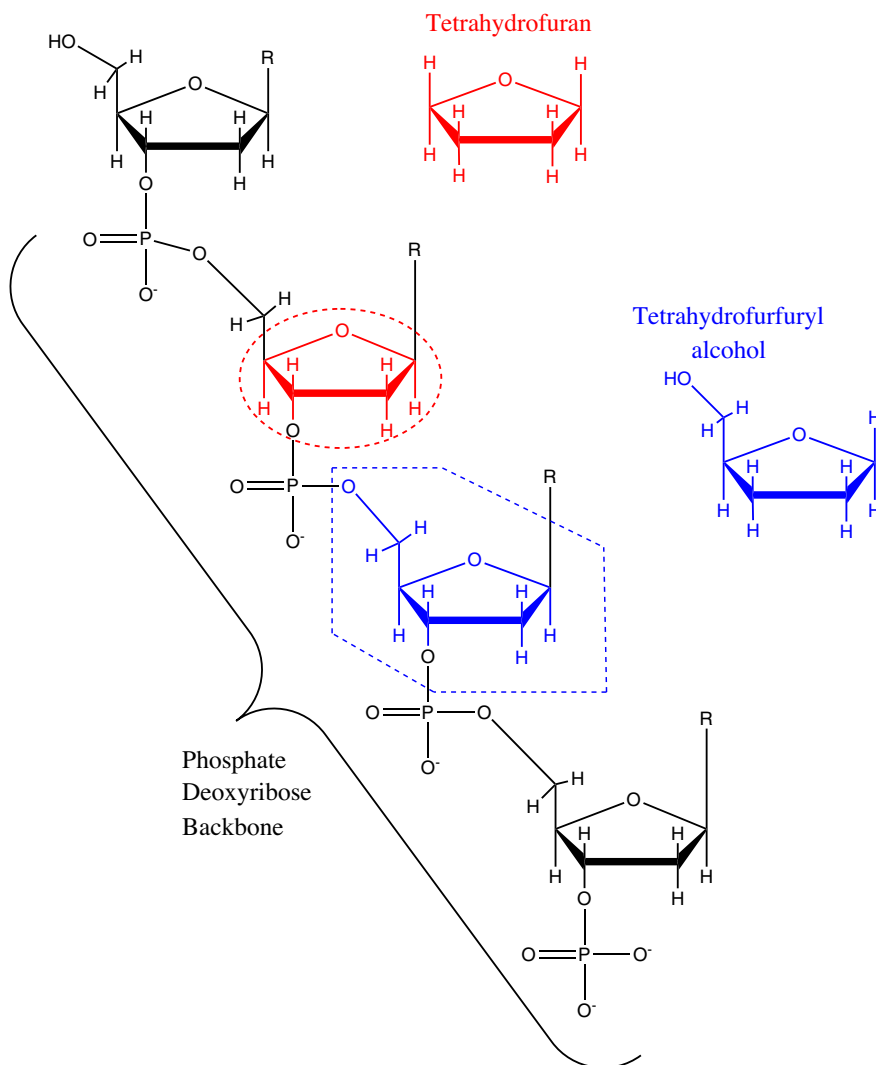


**Figure 1.** Schematic diagram of tetrahydrofuran (THF) and tetrahydrofurfuryl alcohol (THFA) as structural analogues to the phosphate deoxyribose backbone found in DNA.

scattering cross sections and dissociative electron-attachment processes [24,25]. Furthermore, Colyer et al. [26–28] have also performed triple differential cross section (TDCS) measurements for the electron-impact ionization of the highest occupied molecular orbital (HOMO) of THF under asymmetric coplanar kinematics. In that body of work [26–28] angular distributions of the ejected electron, with energy  $E_b = 10$  eV, were measured for the electron-impact ionization of the HOMO when the scattered electron was detected at the angles of  $\theta_a = -5^\circ, -10^\circ$  or  $-15^\circ$ , respectively, while the incident electrons energy was  $E_0 = 250$  eV. Recently, we performed an electron-impact ionization study of the HOMO of THFA (28a) under similar asymmetric coplanar kinematics [29], although in that study the angular distributions of the ejected electron were measured for an ejected electron energy of 20 eV while the scattered electron was again detected at  $\theta_a = -5^\circ, -10^\circ$  or  $-15^\circ$ . Most noticeably, the measurements for both THFA and THF showed significant recoil peak intensity when the scattered electron was detected at  $\theta_a = -5^\circ$ . This observation is intriguing as it suggests that the behavior for electron-impact ionization of the HOMOs for THF and THFA may be similar. This result may however be rationalized as the ionized orbitals in both cases are expected to be dominated by contributions from the lone-electron pair located on the oxygen atom forming the five-member ring. We note in this context, that the HOMO for conformationally versatile THF is either the  $12a'$

(a)  $E_0 = 250$  eV,  $\theta_a = -5^\circ$ ,  $E_b = 20$  eV (b)  $E_0 = 250$  eV,  $\theta_a = -5^\circ$ ,  $E_b = 10$  eV

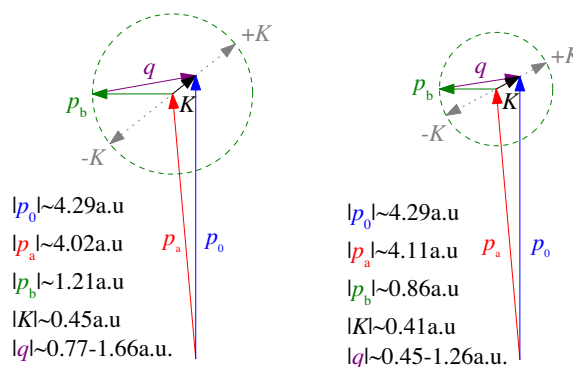


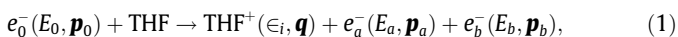
**Figure 2.** Schematic diagram of the kinematics employed for the TDCS measurements of (a) THF (present work) and THFA [29] and (b) THF (work of Colyer et al. [26]). The dashed line in each figure displays the range of ejected electron momentum values with the variation in polar angles. See text for further details.

( $C_s$ ) or  $9b$  ( $C_2$ ) orbital. Nonetheless, the different kinematical conditions employed in the THF [26–28] and THFA [29] measurements (see Figure 2) restrict our ability to fully differentiate between the

role of structure and kinematics in the electron-impact ionization phenomena. To resolve this issue, we have thus performed new measurements for THF under kinematical conditions that match those employed for our recent measurements on THFA [29]. Specifically, angular distributions for  $E_0 = 250$  eV and 20 eV ejected electrons were measured while the detected scattered electron angle was fixed at  $\theta_a = -5^\circ$ . By comparing the new TDCS measurements to the earlier measurements of THF [26] we can gain insights into the sensitivity of the electron-impact cross section to the ejected electron energy. Further, we can make a direct comparison of the new measurements with the existing data for THFA [29] to understand the importance of the exocyclic hydroxyl group in the scattering dynamics.

## 2. Experimental methods and theoretical details

Triple differential cross sections for the kinematically-complete electron-impact ionization of THF, described by



have been measured under coplanar asymmetric kinematical conditions using a (e,2e) coincidence technique. In Eq. (1),  $E_j$  and  $\mathbf{p}_j$  ( $j = 0, a$  or  $b$ ) are the energies and momenta of the incident, scattered and ejected electrons, respectively. Here the conservation of energy during the collision allows the binding energy of the ionized orbital ( $\epsilon_i$ ) to be determined,

$$\epsilon_i = E_0 - (E_a + E_b). \quad (2)$$

Likewise, to conserve momentum the recoiling ion has momentum

$$\mathbf{q} = \mathbf{p}_0 - (\mathbf{p}_a + \mathbf{p}_b), \quad (3)$$

after the collision. The direction of the scattered electron defines the momentum transferred to the target,

$$\mathbf{K} = \mathbf{p}_0 - \mathbf{p}_a. \quad (4)$$

Under the conditions where the electron is ejected in a direction close to the momentum transfer direction ( $+K$ ), all momentum transferred to the target is absorbed by the outgoing electron. In this region the magnitude of the momentum of the recoiling ion is at its minimum, and the collisions are said to be binary. When the electron is ejected in the direction anti-parallel to the momentum transfer ( $-K$ ), however, substantial momentum may be transferred to the recoiling ion. The recoil momentum is then near its maximum, and the collisions are said to be recoil in nature.

The full details of our experimental apparatus and measurement procedure have been described previously [26,30], so that only a brief summary is presented here. An electron beam of fixed energy,  $E_0 = 250$  eV, is generated with an electron gun consisting of a tungsten filament and a 5-element cylindrical lens stack. In the scattering region, the electron beam crosses a beam of high-purity THF, degassed by repeated freeze-pump-thaw cycles, introduced into the system by a capillary. During the measurements, the vacuum chamber and sample gas lines were heated to  $\sim 40^\circ\text{C}$ . Scattered and ejected electrons produced through ionizing collisions with the target beam were detected in separate analyzers. Using standard coincidence timing techniques, the arrival times of the electrons detected in each analyzer were used to determine if the electrons originated from the same ionization event. In this study the obtained binding energy resolution was 1.1 eV (FWHM), as determined from measurements of the Helium 1s binding energy peak. To obtain the coincidence angular distribution of the ejected electron, the scattered electron analyzer was fixed at  $\theta_a = -5^\circ$ , while the ejected electron analyzer was rotated in the scattering plane.

The present experimental data is compared to theoretical calculations obtained within a M3DW (molecular 3-body distorted wave) framework [31–33]. These calculations have been described elsewhere, so only a brief description is repeated here. The TDCS for the M3DW is given by

$$\frac{d\sigma}{d\Omega_a d\Omega_b dE_b} = \frac{1}{(2\pi)^5} \frac{k_a k_b}{k_i} (|T_{dir}|^2 + |T_{exc}|^2 + |T_{dir} - T_{exc}|^2), \quad (5)$$

where  $\vec{k}_i$ ,  $\vec{k}_a$ , and  $\vec{k}_b$  are the wave vectors for the initial, scattered and ejected electrons, respectively,  $T_{dir}$  is the direct scattering amplitude, and  $T_{exc}$  is the exchange amplitude. The direct scattering amplitude is given by

$$T_{dir} = \left\langle \chi_i^-(\vec{k}_a, \mathbf{r}_1) \chi_b^-(\vec{k}_b, \mathbf{r}_2) C_{scat-eject}(r_{12}^{ave}) | V - U_i | \phi_{DY}^{OA}(\mathbf{r}_2) \chi_i^+(\vec{k}_i, \mathbf{r}_1) \right\rangle, \quad (6)$$

here  $\mathbf{r}_1$  and  $\mathbf{r}_2$  are the coordinates of the incident and the bound electrons,  $\chi_i$ ,  $\chi_a$ , and  $\chi_b$  are the distorted waves for the incident, scattered, and ejected electrons respectively, and  $\phi_{DY}^{OA}(\mathbf{r}_2)$  is the initial bound-state Dyson molecular orbital averaged over all orientations. Under the frozen orbital approximation, the Dyson orbital can be approximated using the initial bound Kohn–Sham orbital. The molecular wave functions were calculated using density functional theory (DFT) along with the standard hybrid B3LYP [34] functional by means of the ADF 2007 (Amsterdam Density Functional) program [35] with the TZ2P (triple-zeta with two polarization functions) Slater type basis sets. The factor  $C_{scat-eject}(r_{12}^{ave})$  is the Ward–Macek average Coulomb-distortion factor between the two final state electrons [36],  $V$  is the initial state interaction potential between the incident electron and the neutral molecule, and  $U_i$  is a spherically symmetric distorting potential which is used to calculate the initial-state distorted wave for the incident electron  $\chi_i^+(\vec{k}_i, \mathbf{r}_1)$ . For the exchange amplitude  $T_{exc}$ , particles 1 and 2 are interchanged in Eq. (6).

The Schrödinger equation for the incoming electron wave-function is given by:

$$\left( T + U_i - \frac{k_i^2}{2} \right) \chi_i^+(\vec{k}_i, r) = 0, \quad (7)$$

where  $T$  is the kinetic energy operator and the ‘+’ superscript on  $\chi_i^+(\vec{k}_i, r)$  indicates outgoing wave boundary conditions. The initial state distorting potential contains three components  $U_i = U_s + U_E + U_{CP}$ , where  $U_s$  contains the nuclear contribution plus a spherically symmetric approximation for the interaction between the projectile electron and the target electrons which is obtained from the quantum mechanical charge density of the target. The charge density is obtained by summing  $2|\phi_{DY}|^2$  over all occupied orbitals (the 2 is for double occupancy and the original non-averaged Dyson orbital is used). The nuclear contribution to  $U_s$  is the interaction between the projectile electron and all the 17 nuclei averaged over all orientations. Averaging the nuclei over all orientations is equivalent to putting the nuclear charge on a thin spherical shell whose radius is the distance of the nuclei from the center of mass (CM). For THF, there is no nucleus at the CM and the 4 carbon nuclei and one oxygen nucleus are all about the same distance from the CM. The closest nucleus to the CM is the oxygen at  $2.35 a_0$ . Consequently, the first nuclear sphere has a charge of 8 with a radius of  $2.35 a_0$ . The next sphere has 2 carbon nuclei with charge 12 and a radius of  $2.36 a_0$ . The next sphere has another 2 carbon nuclei with charge 12 and a radius of  $2.37 a_0$ . The 8 hydrogen nuclei are on 4 spheres of charge 2 located at 3.69, 3.75, 4.10, and  $4.21 a_0$  respectively.  $U_E$  is the exchange potential of Furness–McCarthy (corrected for sign errors) [37] which approximates the effect of the continuum electron exchanging with the passive bound electrons in the molecule, and

$U_{CP}$  is the correlation-polarization potential of Perdew and Zunger [38] (see also Padial and Norcross [39]).

In Eq. (6), the final state for the system is approximated as a product of distorted waves for the two continuum electrons ( $\chi_a^-, \chi_b^-$ ) times the Ward–Macek average Coulomb-distortion factor  $C_{scat-eject}$ . The final state distorted waves are calculated the same as the initial state except that the final state charge density is used to calculate  $U_s$ . The final state charge density is obtained the same as the initial state except that unity occupancy is used for the active electron orbital. Additional details can be found in Madison and Al-Hagan [40].

In order to offer more quantitative comparisons between THF and THFA, the calculated TDCS for THF are weighted by a 1:1,  $C_1:C_2$  conformer ratio that is close to the recently observed experimental values [41–43] at room temperature, and is thus representative of the conditions used in our experiments. Lastly, in order to facilitate further quantitative understanding of the observed behavior, spherically averaged orbital momentum profiles have been generated [44] for both THF and THFA from Kohn–Sham orbitals calculated with GAUSSIAN [45].

### 3. Results and discussion

In Figure 3, the newly measured binding energy spectrum (BES) for THF is presented. This spectrum was obtained for an incident electron energy  $E_0 = 250$  eV, with the scattered electron being detected at  $\theta_a = -10^\circ$  in coincidence with an ejected electron with  $E_b = 20$  eV at  $\theta_b = 75^\circ$ . Here the data is accumulated by recording the number of true coincident events as the scattered electron energy was scanned. Note that the features observed in this spectrum are in good accord with results obtained in ultraviolet photoelectron spectroscopy (UPS) [46,47], Penning ionization electron spectroscopy (PIES) [47], and electron momentum spectroscopy [42,43]. Interestingly, the BES from the earlier dynamical (e,2e) study [26] shows marked differences to the present spectra. Here those variations relate to the relative intensity of each spectral feature, which highlights the importance of the kinematical conditions to the spectral behavior. Specifically, the BES of Colyer et al. (Figure 3 of Ref. [26]) and the present spectrum are obtained in

the binary region with recoil momentum values,  $|q|$ , of  $\sim 0.3$  and  $\sim 0.5$  a.u., respectively. The shift from a low to higher recoil momentum value probes different parts of the momentum profile of the ionized orbital. As such, the nature of the ionized orbitals momentum profile dramatically influences the relevant state's contribution to the spectrum [48].

In Figure 4 (a), measured TDCS for the HOMO of THF ( $12a' + 9b$ ) are presented for  $\theta_a = -5^\circ$  and  $E_b = 20$  eV. Initially, we compare the present TDCS for THF shown in Figure 4 (a) with the results measured previously for THF under different kinematics, i.e.  $E_b = 10$  eV, (Figure 5 of Ref. [26]). Here we see a significant reduction in the observed binary to recoil ratio as the ejected electron's energy has increased from 10 to 20 eV. Comparing these results with those from the M3DW calculations, we see that the theory gives a much better prediction of the shape of the binary feature when the ejected electron energy is 20 eV. However, the M3DW still fails to reproduce the significant recoil peak intensity observed experimentally in both this work and that of Colyer et al. [26].

In order to qualitatively understand this behavior, we expand on the ideas proposed by Xu et al. [48]. Here we make reference to the kinematical conditions detailed in Figure 2 and the momentum profiles for the HOMO ( $12a'$ ,  $9b$  and conformational averaged  $12a' + 9b$ ) of THF which are presented in Figure 5. In both measurements the momentum transfer is small, being  $\sim 0.4$  a.u. However, this momentum transfer is significantly less than the outgoing electrons momentum, being  $|p_b| = 0.86$  and  $1.21$  a.u. for  $E_b = 10$  eV and  $20$  eV, respectively. The ionization process must therefore always rely on linear momentum contributions from the internal momentum of the particles within the target. Note that in the impulsive limit, where no momentum is transferred to the recoiling ion, the momentum of the ionized electron is equal and opposite to the recoil momentum (this is the so-called electron momentum spectroscopy experiment [49]). The momentum profile and recoil momentum magnitude may therefore have a large influence on the scattering dynamics.

In the two kinematical conditions with  $E_b = 10$  or  $20$  eV the magnitude of the recoil momentum belongs to the ranges of  $0.45$ – $1.26$  and  $0.77$ – $1.66$  a.u., respectively. As the THF  $12a' + 9b$  momentum profile has a minimum at  $|q| \sim 0.4$  a.u. and a maximum at  $|q| \sim 1.0$  a.u. we may expect a weak intensity for the binary peak

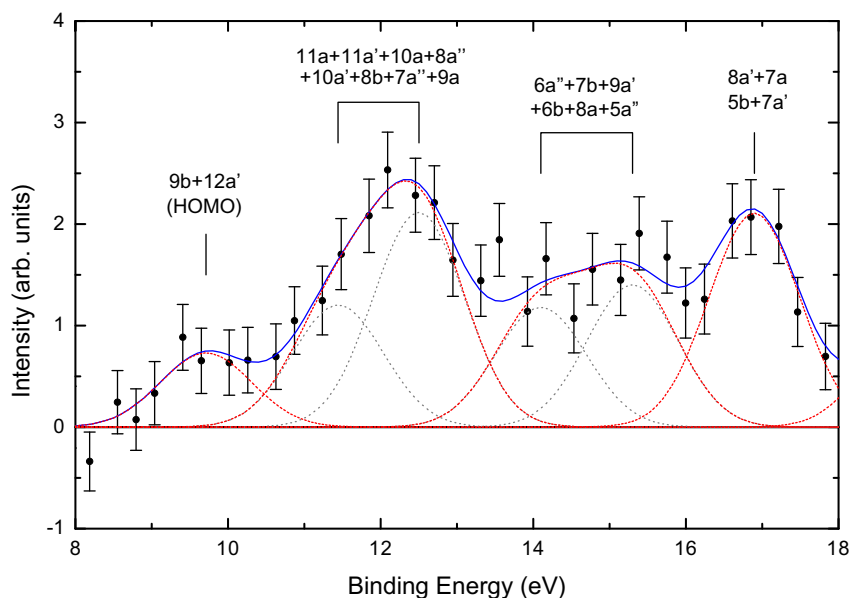


**Figure 3.** Binding energy spectrum for THF obtained for an incident electron energy  $E_0 = 250$  eV. Measured experimental data ( $\bullet$ ). Here the scattered electron was detected at  $\theta_a = -10^\circ$ , while the ejected electron was detected with  $E_b = 20$  eV at  $\theta_b = 75^\circ$ . Also shown are spectral deconvolutions of the measured spectra into contributions from each orbital (---) and their sum (—). Also shown are the individual (unresolved) Gaussians (.....) that combine to form the larger spectral features. See text for further details.

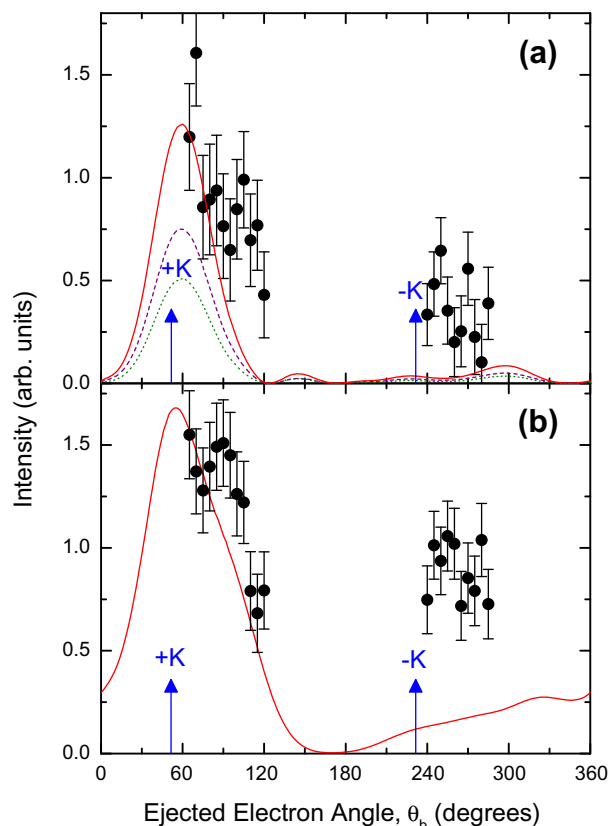


**Figure 4.** Triple differential cross sections for the electron-impact ionization of the HOMOs of (a) THF (9b + 12a') and (b) THFA (28a) [29], with  $E_0 = 250$  eV, at  $\theta_a = -5^\circ$ , and  $E_b = 20$  eV. Measured experimental data ( $\bullet$ ). The M3DW calculations (—) are also presented for each orbital or conformational average of contributing orbitals. Also shown are the TDCS contributions from the 12a' (---) and 9b (.....) orbitals of THF after being weighted by their respective conformer populations. See text for further details.

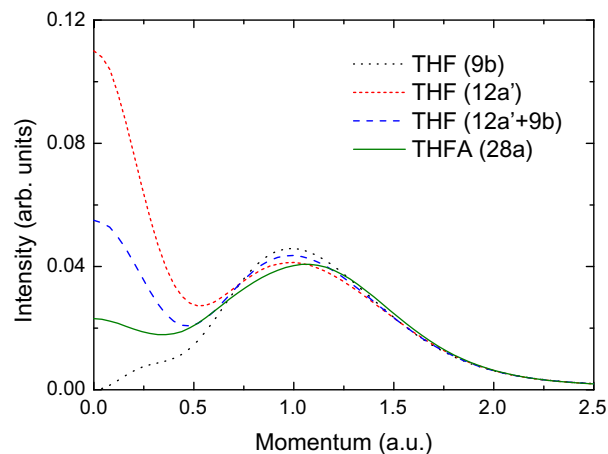


**Figure 5.** Momentum profiles for the HOMOs (9b, 12a' and conformationally averaged 9b + 12a') of THF and 28a of THFA. See text for further details.

and a more significant recoil peak for  $E_b = 10$  eV. Conversely, under conditions where the ejected electron leaves with 20 eV, the maximum in the momentum profile coincides with the recoil momentum value when the electron is ejected along the momentum transfer direction. The TDCS should therefore be at its maximum in this binary region. As the momentum distribution decreases in

going to higher recoil momentum values, it might be expected that the recoil peak intensity is reduced from that found in the binary region for  $E_b = 20$  eV. Such observations are consistent with the experimental binary-to-recoil ratios observed by Colyer et al. [26] and in the present work. Thus, the behavior of the momentum profile over the recoil momentum values studied through the defined kinematics provides a qualitative rationale for the experimentally observed binary-to-recoil peak ratios.

The TDCS for THF and THFA, measured under identical scattering conditions and shown in Figure 4(a) and (b), are now discussed. It is immediately apparent from Figure 4 that the recoil peak for THF is somewhat smaller than that observed previously for THFA. Specifically, the recoil peak of THF is roughly a third of the intensity of the binary peak while for THFA the recoil peak is about half the intensity measured for the binary peak. This behavior is somewhat surprising as the HOMOs for both THF and THFA are structurally expected to be quite similar. Indeed, the momentum profiles of the HOMOs of both THF and THFA, shown in Figure 5, are essentially identical over the range of recoil momentum values covered by the relevant kinematical conditions,  $|\mathbf{q}| \sim 0.8\text{--}1.7$  a.u., of both experiments. With the identical kinematical conditions, the observed variation in the binary-to-recoil ratios suggests that the dynamics of the ionization process must clearly influence the scattering behavior. In this respect, comparisons between M3DW and distorted-wave Born approximation calculations for both THF (not shown) and THFA [29] have revealed that post-collision interactions between the two outgoing electrons are unimportant under the present kinematics. This perhaps suggests that a better description of the post-collisional interaction between the two outgoing electrons and the residual ion may therefore be required.

#### 4. Conclusions

By supplementing earlier studies on electron-impact ionization of THF [26], with new experimental measurements and theoretical calculations under kinematical conditions that matched those employed in our previous study of THFA [29], significant insights into the nature of the observed binary-to-recoil ratios have been revealed. The present results for THF, when compared against previous results measured under different kinematical conditions [26], suggest that the relevant orbital momentum profiles may assist us in understanding the observed binary-to-recoil peak ratios for a particular target. However, when the TDCS measurements of THF were compared to those from THFA, it was also apparent that a quantitative understanding of the collision dynamics is also required to explain the observed scattering phenomena.

#### Acknowledgements

This research was supported by the Australian Research Council (ARC) Centre of Excellence for Antimatter-Matter Studies, by the US National Science Foundation under Grant No. PHY-1068237 (H.C. and D.H.M.), and by the National Natural Science Foundation of China under Grant No. 11174175 (C.G.N.). D.B.J. acknowledges financial support provided through an ARC Discovery Early Career Researcher Award (DECRA). O.I. acknowledges support from the Icelandic Centre for Research (RANNIS) and the Research fund of the University of Iceland.

#### References

- [1] L. Chiari, M.J. Brunger, A. Zecca, Total cross sections for positron scattering from bio-molecules, in: G. Garcia Gomez-Tejedor, M.C. Fuss (Eds.), *Radiation Damage in Biomolecular Systems*, Springer, London, UK, 2012, pp. 155–163.
- [2] I. Baccarelli, I. Bald, F.A. Gianturco, E. Illenberger, J. Kopyra, *Phys. Rep.* 508 (2011) 1.
- [3] S.M. Pimblott, J.A. LaVerne, *Radiat. Phys. Chem.* 76 (2007) 1244.

- [4] B. Boudaiffa, P. Cloutier, D. Hunting, M.A. Huels, L. Sanche, *Science* 287 (2000) 1658.
- [5] X. Pan, P. Cloutier, D. Hunting, L. Sanche, *Phys. Rev. Lett.* 90 (2003) 208102.
- [6] F. Martin, P.D. Burrow, Z.L. Cai, P. Cloutier, D. Hunting, L. Sanche, *Phys. Rev. Lett.* 93 (2004) 068101.
- [7] D.S. Milne-Brownlie, S.J. Cavanagh, B. Lohmann, C. Champion, P.A. Hervieux, J. Hanssen, *Phys. Rev. A* 69 (2004) 032701.
- [8] C.J. Colyer, M.A. Stevenson, O. Al-Hagan, D.H. Madison, C.G. Ning, B. Lohmann, *J. Phys. B: At. Mol. Opt. Phys.* 42 (2009) 235207.
- [9] J. Builth-Williams, S.M. Bellm, D.B. Jones, H. Chaluvadi, D. Madison, C.G. Ning, B. Lohmann, M.J. Brunger, *J. Chem. Phys.* 136 (2012) 024304.
- [10] S.M. Bellm, C.J. Colyer, B. Lohmann, C. Champion, *Phys. Rev. A* 85 (2012) 022710.
- [11] A. Zecca, L. Chiari, G. Garcia, F. Blanco, E. Trainotti, M.J. Brunger, *New J. Phys.* 13 (2011) 063019.
- [12] A. Zecca, C. Perazzolli, M.J. Brunger, *J. Phys. B: At. Mol. Opt. Phys.* 38 (2005) 2079.
- [13] M. Fuss, A. Munoz, J.C. Oller, F. Blanco, D. Almeida, P. Limão-Vieira, T.P.D. Do, M.J. Brunger, G. Garcia, *Phys. Rev. A* 80 (2009) 052709.
- [14] P. Mozejko, E. Ptasinska-Denga, A. Domaracka, C. Szmytkowski, *Phys. Rev. A* 74 (2006) 012708.
- [15] W.Y. Baek, M. Bug, H. Rabus, E. Gargioni, B. Grosswendt, *Phys. Rev. A* 86 (2012) 032702.
- [16] C.J. Colyer, V. Vizcaino, J.P. Sullivan, M.J. Brunger, S.J. Buckman, *New J. Phys.* 9 (2007) 41.
- [17] A.R. Milosavljevic, A. Giuliani, D. Sevic, M.J. Hubin-Franskin, B.P. Marinkovic, *Eur. Phys. J. D* 35 (2005) 411.
- [18] M. Dampc, A.R. Milosavljević, I. Linert, B.P. Marinković, M. Zubek, *Phys. Rev. A* 75 (2007) 042710.
- [19] A.R. Milosavljević, F. Blanco, D. Šević, G. García, B.P. Marinković, *Eur. Phys. J. D* 40 (2006) 107.
- [20] A. Gauf, L.R. Hargreaves, A. Jo, J. Tanner, M.A. Khakoo, T. Walls, C. Winstead, V. McKoy, *Phys. Rev. A* 85 (2012) 052717.
- [21] M. Allan, *J. Phys. B: At. Mol. Opt. Phys.* 40 (2007) 3531.
- [22] T.P.T. Do, M. Leung, M. Fuss, G. Garcia, F. Blanco, K. Ratnavelu, M.J. Brunger, *J. Chem. Phys.* 134 (2011) 144302.
- [23] M. Dampc, I. Linert, A.R. Milosavljević, M. Zubek, *Chem. Phys. Lett.* 443 (2007) 17.
- [24] B.C. Ibanescu, O. May, A. Monney, M. Allan, *Phys. Chem. Chem. Phys.* 9 (2007) 3163.
- [25] P. Sulzer, S. Ptasinska, F. Zappa, B. Mielewska, A.R. Milosavljevic, P. Scheier, T.D. Mark, I. Bald, S. Gohlke, M.A. Huels, E. Illenberger, *J. Chem. Phys.* 125 (2006) 044304.
- [26] C.J. Colyer, S.M. Bellm, B. Lohmann, G.F. Hanne, O. Al-Hagan, D.H. Madison, C.G. Ning, *J. Chem. Phys.* 133 (2010) 124302.
- [27] C.J. Colyer, S.M. Bellm, G.F. Hanne, O. Al-Hagan, D. Madison, C.G. Ning, B. Lohmann, *J. Phys. Conf. Ser.* 288 (2011) 012007.
- [28] C.J. Colyer, M.A. Stevenson, B. Lohmann, *J. Phys.: Conf. Ser.* 194 (2009) 052022.
- [29] S.M. Bellm, J.D. Builth-Williams, D.B. Jones, H. Chaluvadi, D.H. Madison, C.G. Ning, F. Wang, X.G. Ma, B. Lohmann, M.J. Brunger, *J. Chem. Phys.* 136 (2012) 244301.
- [30] S.J. Cavanagh, B. Lohmann, *J. Phys. B: At. Mol. Opt. Phys.* 32 (1999) L261.
- [31] J. Gao, D.H. Madison, J.L. Peacher, *J. Chem. Phys.* 123 (2005) 204314.
- [32] J. Gao, D.H. Madison, J.L. Peacher, *J. Phys. B: At. Mol. Opt. Phys.* 39 (2006) 1275.
- [33] J. Gao, J.L. Peacher, D.H. Madison, *J. Chem. Phys.* 123 (2005) 204302.
- [34] C. Lee, W. Yang, R.G. Parr, *Phys. Rev. B* 37 (1988) 785.
- [35] C.F. Guerra, J.G. Snijders, G. te Velde, E.J. Baerends, *Theor. Chem. Acc.* 99 (1998) 391.
- [36] S.J. Ward, J.H. Macek, *Phys. Rev. A* 49 (1994) 1049.
- [37] J.B. Furness, I.E. McCarthy, *J. Phys. B: Atom. Molec. Phys.* 6 (1973) 2280.
- [38] J.P. Perdew, A. Zunger, *Phys. Rev. B* 23 (1981) 5048.
- [39] N.T. Padiyal, D.W. Norcross, *Phys. Rev. A* 29 (1984) 1742.
- [40] D.H. Madison, O. Al-Hagan, *J. At. Mol. Opt. Phys.* 2010 (2010) 367180.
- [41] A. Giuliani, P. Limão-Vieira, D. Duflo, A.R. Milosavljevic, B.P. Marinkovic, S.V. Hoffmann, N. Mason, J. Delwiche, M.J. Hubin-Franskin, *Eur. Phys. J. D* 51 (2009) 97.
- [42] C.G. Ning, Y.R. Huang, S.F. Zhang, J.K. Deng, K. Liu, Z.H. Luo, F. Wang, *J. Phys. Chem. A* 112 (2008) 11078.
- [43] T. Yang, G. Su, C. Ning, J. Deng, F. Wang, S. Zhang, X. Ren, Y. Huang, *J. Phys. Chem. A* 111 (2007) 4927.
- [44] J.P.D. Cook, C.E. Brion, *Chem. Phys.* 69 (1982) 339.
- [45] M.J. Frisch et al., GAUSSIAN 09, Revision B.01, Gaussian Inc., Wallington CT, USA (2010).
- [46] K. Kimura, S. Katsuwata, Y. Achiba, T. Yamazaki, S. Iwata, *Handbook of Hel Photoelectron Spectra of Fundamental Organic Molecules*, Japan Scientific Societies Press, Tokyo, Japan, 1981.
- [47] M. Yamauchi, H. Yamakado, K. Ohno, *J. Phys. Chem. A* 101 (1997) 6184.
- [48] S. Xu, X. Ma, S. Yan, P. Zhang, *J. Chem. Phys.* 136 (2012) 237101.
- [49] E. Weigold, I.E. McCarthy, *Electron Momentum Spectroscopy*, Kluwer Academic/Plenum Publishers, New York, 1999.